Low Reynolds number wake modification using a Gurney flap

Muralikrishnan Gopalakrishnan Meena* and Kunihiko Taira†

Florida State University, Tallahassee, FL 32310, USA

Keisuke Asai[‡]

Tohoku University, Sendai, Miyagi 980-8577, Japan

We numerically examine the use of Gurney flap to modify the two-dimensional wake dynamics for lift enhancement on NACA 0000 (flat plate), 0006, 0012 and 0018 airfoils. Incompressible flows over the airfoils at different angles of attack are considered at Re=1000. It is observed that the attachment of the Gurney flap at the trailing edge is able to enhance the lift force experienced by the airfoil appreciably with increase in Gurney flap height. The lift-to-drag ratio of the airfoils is also observed to increase at lower angles of attack. The lift spectra and airfoil wake are examined to reveal the effect of the Gurney flap on the formation of different characteristic wake modes and the associated change in the aerodynamic forces exerted on the airfoils. Based on the observations, we classify the resulting wakes into four distinct modes. The emergence of these modes (steady, 2S, P and 2P) are mapped over a wide range of angles of attack and Gurney flap heights for all four airfoils in consideration.

Nomenclature

- Re Chord based Reynolds number
- u_{∞} Free stream velocity
- c Airfoil chord length
- l* Characteristic frontal length
- ν Kinematic viscosity
- ρ Fluid density
- h Gurney flap height
- α Angle of attack
- C_D Coefficient of drag
- C_L Coefficient of lift
- St Strouhal number
- F_x Drag on airfoil
- F_{y} Lift on airfoil
- f_s Vortex shedding frequency
- ω Vorticity

 $^{^*}$ Graduate Research Assistant, Department of Mechanical Engineering and Florida Center for Advanced Aero-Propulsion, Florida State University, mg15h@my.fsu.edu, Student Member AIAA

[†]Assistant Professor, Department of Mechanical Engineering and Florida Center for Advanced Aero-Propulsion, Florida State University, ktaira@fsu.edu, Associate Fellow AIAA

[‡]Professor, Department of Aerospace Engineering, Tohoku University, Associate Fellow AIAA

I. Introduction

The versatility of micro air vehicles (MAV) to perform a wide range of missions have led to their growing popularity in recent years. Flight operation of such vehicles in regimes of insects and birds make MAVs fly at low Reynolds number of $Re = O(10^3 - 10^4)$ under the influence of vortical flows. Thus it is vital to design, develop and test MAVs in flow conditions experienced by insects, birds and the aforementioned environments at low Reynolds numbers. Moreover, wings used by MAVs should acquire significant aerodynamic performance at high angle of attack to achieve a wide flight envelope and to tackle unsteady wind gusts and disturbances. As a means to enhance the aerodynamic performance of airfoils, we examine the use of Gurney flaps, which is a high-lift generating flow control device that has been in use over a few decades.¹⁻⁹ The simple nature of Gurney flaps make it an attractive choice of implementation in low Reynolds number airfoil for flow control. The majority of the past research focus on the use of Gurney flaps for high Reynolds number, where $Re = O(10^4 - 10^6)$.¹⁻⁹ In contrast, there appears to be limited applications of the flaps for wings at low Reynolds number of $Re = O(10^3)$.

Early studies on flow over airfoils at Re=1000 were conducted by Mittal and Tezduyar.¹⁰ Finite element computations were performed for unsteady incompressible flows past NACA 0012 airfoil. Flow patterns and aerodynamic forces were analyzed for a stationary airfoil. Recently, Kurtulus^{11,12} numerically studied flow over a stationary NACA 0012 airfoil at Re=1000 for a wide range of angle of attacks from 0° to 90°. Wake patterns and unsteady aerodynamic forces were analyzed to understand post-stall vortex formation and flow separation. One of the few available literature on incompressible flow over airfoils with Gurney flap at Re=1000 was conducted numerically by Mateescu et al.¹³ Symmetric and cambered NACA airfoils with Gurney flap attached to the trailing edge were analyzed by the authors. A basic knowledge about the flow physics and aerodynamic forces were also reported. The physics governing the flow control phenomena involved when Gurney flaps are attached or deployed at the trailing edge of airfoils at high Re flows is examined in the aforementioned papers. On the contrary, the availability of such literature is limited for low Re cases. Moreover, the behavior of far field wake structure for both low as well as high Re flows are not well documented.

In the present work, we perform a large parametric study to examine the influence of Gurney flap on the aerodynamic characteristic and wake patterns behind NACA 0000, 0006, 0012 and 0018 airfoils. In the following section, the computational approach and setup for the study is described. This is followed by the discussion of results in Section III, where we first classify the four characteristic wake modes observed. We then examine the effects of the Gurney flap on lift, drag and lift-to-drag ratio for all airfoils. The spectral analysis of the lift history are provided as additional information in the Appendix.

II. Computational Approach

We investigate the influence of Gurney flaps on the two-dimensional wake behind four different symmetric airfoils, NACA 0000 (flat plate), 0006, 0012 and 0018 at a chord-based Reynolds number of $Re \equiv u_{\infty}c/\nu = 1000$. Wide range of values for the Gurney flap height and angle of attack are considered in this study as shown in figure 1(a). The flow field and force data obtained for each case are analyzed in detail to acquire a knowledge on the underlying effect of flow control implemented on the airfoils for aerodynamic performance enhancement.

For the current analysis, the immersed boundary projection method^{14,15} is used to simulate the flow. This method is based on a finite volume formulation and incorporates the no-slip boundary condition along the immersed boundary into the projection operation. The scheme is second-order accurate in time and has a spatial accuracy of 1.5 in space. Moreover, a multi-domain technique is used to simulate flow over a body in free space. The scheme has been validated for a number of cases, and has been found robust and accurate.¹⁵

Figure 1(a) depicts the problem setup for the current work. Throughout the paper, the length scale is non-dimensionalized by the chord length c, time by convective time scale c/u_{∞} and velocity by the free stream velocity u_{∞} . Angles of attack α between 0° to 20° are considered for all the airfoils, of which Gurney flap is attached to the trailing edge perpendicular to the chord line. For all cases, Gurney flap height of h/c between 0 to 0.15 are considered. The wing is placed in the domain with its quarter-chord point at the origin with uniform flow prescribed at the inlet. Five nested levels of multi-domains are used with the finest level being $[-1,1] \times [-1,1]$ and the largest domain being $[-16,16] \times [-16,16]$.

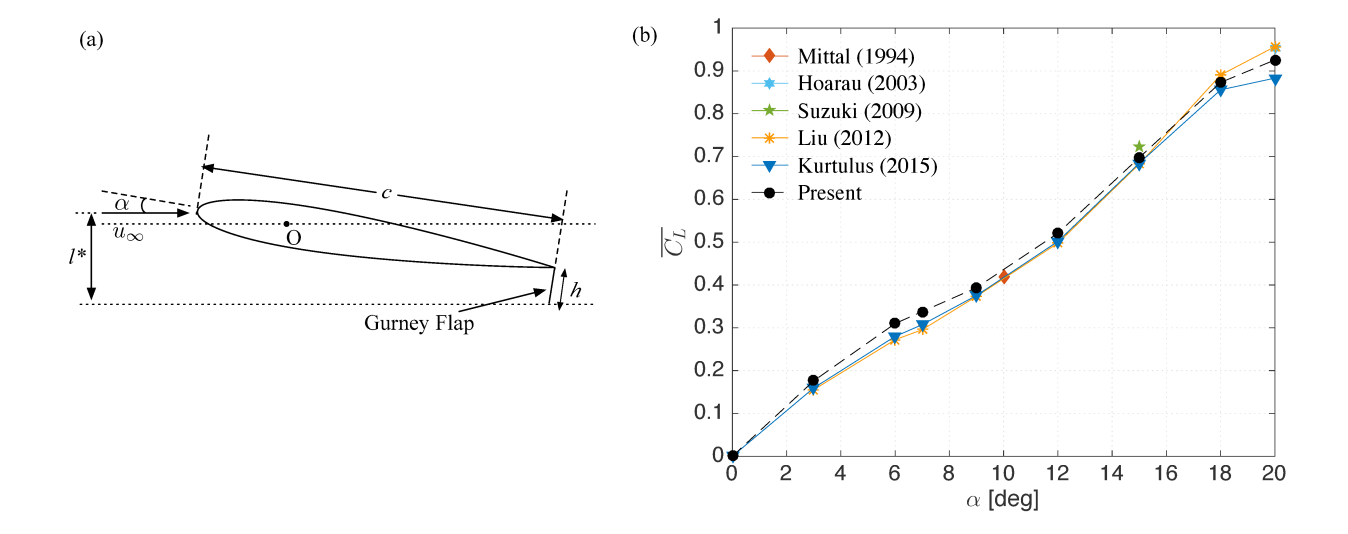


Figure 1. (a) Model profile, NACA 0012 airfoil at $\alpha=9^{\circ}$ with Gurney flap of h/c=0.1 attached to the trailing edge; (b) comparison of mean lift coefficient, $\overline{C_L}$, for NACA 0012 airfoil at Re=1000 with various studies in literature.

In the current study, the drag and lift coefficients are defined as

$$C_D \equiv \frac{F_x}{\frac{1}{2}\rho u_{\infty}^2 c}$$
 and $C_L \equiv \frac{F_y}{\frac{1}{2}\rho u_{\infty}^2 c}$, (1)

respectively. The shedding frequency f_s of lift is non-dimensionalized as the Strouhal number using

$$St \equiv \frac{f_s l^*}{u_{\infty}},\tag{2}$$

where the characteristic frontal length l^* is taken to be

$$l^* = c\sin(\alpha) + h\cos(\alpha),\tag{3}$$

as shown in figure 1(a).

Grid convergence was examined for grid size ranging from 200×200 to 500×500 and a domain with 360×360 grid resolution was found to be sufficient. The time step for all cases is limited to a maximum CFL number of 0.3. Figure 1(b) shows the comparison of mean C_L values of NACA 0012 airfoil at Re = 1000 with past studies. The results obtained from the current simulations are in agreement with the data from literature.

III. Results

We perform a large number of direct numerical simulations of the flow around four different NACA airfoils with and without a Gurney flap attached to the trailing edge. The height of the flap is varied between $h/c \in [0,0.15]$. A significant increase in aerodynamic efficiency of the airfoil is observed with flow control using the Gurney flap. A close examination of the flow field unveils four characteristic wake modes for all the airfoils, both in baseline as well as in cases with Gurney flaps. The flow field and shedding phenomena are studied to understand the aerodynamic characteristics of the airfoil. In the following sections, descriptions on the flow field analysis and the force data are presented. A complete summary on the classification for flow regimes of all cases is also reported.

A. Wake Modes

Let us analyze the vorticity field around the airfoils at Re = 1000 for various Gurney flap heights and angles of attack. We observe four distinct types of wake develop over the airfoil with and without the Gurney flap.

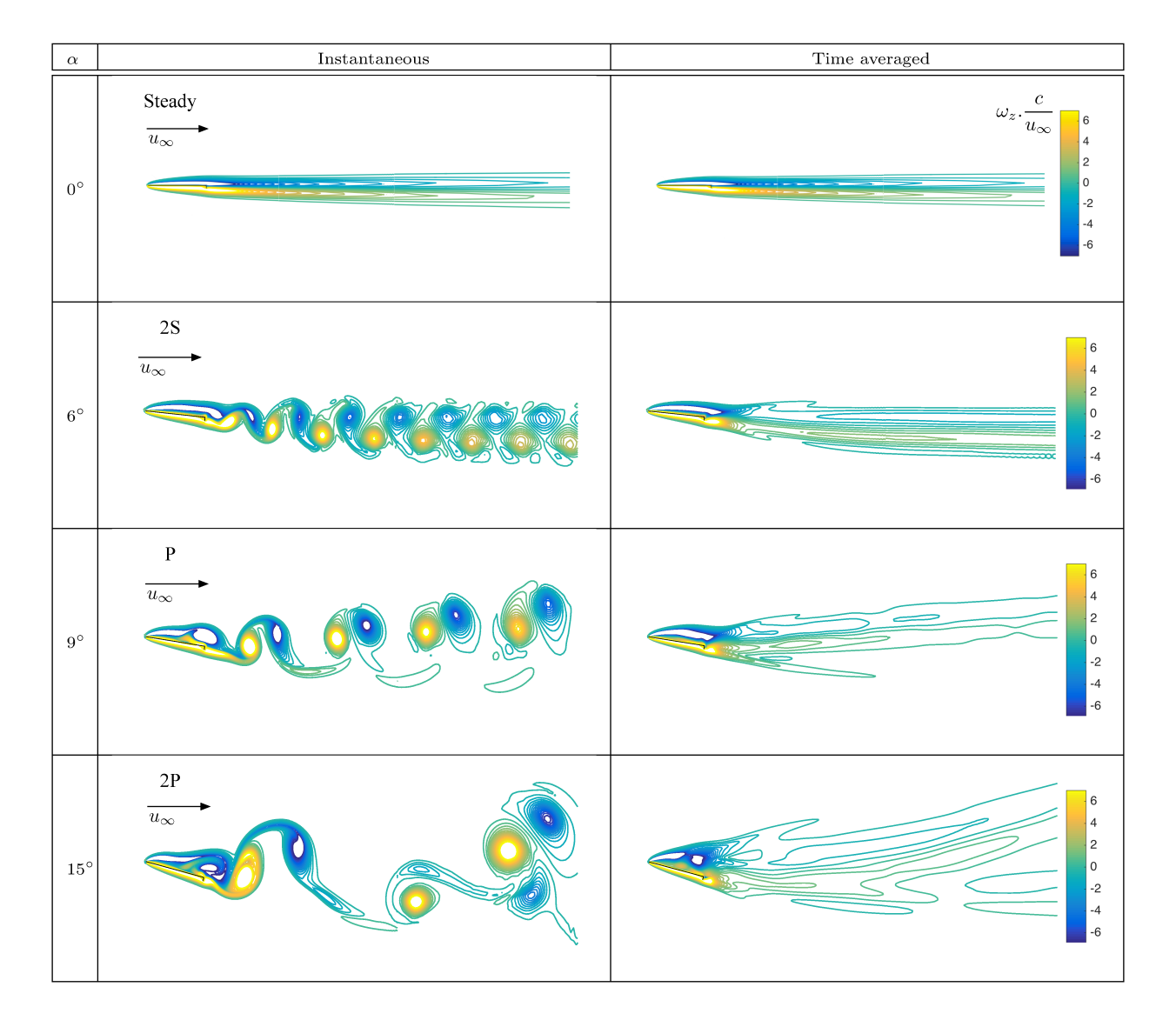


Figure 2. Instantaneous and time averaged vorticity fields $\omega c/u_{\infty}$, around NACA 0000 with a Gurney flap of h/c=0.06 at various α . The contour plots are representative cases portraying the four characteristic regimes: steady, 2S, P and 2P.

The wake transitions from steady to unsteady flow with increase in angle of attack and Gurney flap height. With the addition of Gurney flap and increase of the flap height, the transitions occur at comparatively lower angles of attack. The results show that the flow fields can be characterized into four different regimes depending on the characteristics of vortex shedding.

The far field wake developments of different regimes for a representative airfoil setup (NACA 0000 with h/c = 0.06) are summarized in figure 2. The four types of flow regimes observed are:

- 1. Steady ($\alpha = 0^{\circ}$ case in figure 2)
- 2. 2S periodic von Kármán vortex shedding of alternate counter-clockwise and clockwise rotating vortices ($\alpha = 6^{\circ}$ case)
- 3. P periodic von Kármán shedding of a single vortex pair ($\alpha = 9^{\circ}$ case)
- 4. 2P periodic shedding of two vortex pairs ($\alpha = 15^{\circ}$ case).

These wake modes are classified on the basis of the flow structure of the wake, vortex shedding frequency and force fluctuations. In this section, we discuss the difference in the flow structure of the wake modes. The

nomenclature of the modes follows the wake mode classification performed by Williamson and Roshko¹⁹ for shifting wake modes of an oscillating cylinder. The wake modes observed in the current study are similar to the 2S, P and 2P wake modes defined by Williamson and Roshko. These 2S, P and 2P modes are previously observed in literature for studies involving oscillating cylinder^{19–24} as well as airfoils.^{11,12,25–27} In particular, the wake modes have been observed for the baseline case of NACA 0012 airfoil at Re = 1000 by Kurtulus.^{11,12} Below we discuss each regimes in detail.

In the steady regime (figure 2, $\alpha=0^{\circ}$), the wake is steady and the flow is attached to the airfoil surface. This will attribute to the lowest magnitude of drag experienced by the airfoil compared to that in the other unsteady modes. With increase in α and h/c values, the flow starts to become unsteady. With this, the wake is classified into the next regime, the 2S mode.

The 2S mode (figure 2, $\alpha=6^{\circ}$) is characterized by unsteady flow with periodic von Kármán vortex shedding of alternate clockwise and counter-clockwise rotating vortices (2S represents two single vortices). Shear layer roll up initiates on the airfoil surface. Vortices are shed from the trailing edge of the airfoil, forming a von Kármán vortex street. Also, one will observe peaks in the frequency spectra for the lift force corresponding to the vortex shedding phenomena. The time averaged vorticity contour lines are below the wake centerline. The wake height, observable from the time averaged vorticity fields, is larger compared to that of the steady regime denoting increase in drag experienced by the airfoil. The relatively smaller wake height for the 2S regime compared to the other unsteady regimes is also observed. Detailed description on the aerodynamic forces experienced by the airfoils at different regimes are discussed in Section III B. With further increase in α and h/c values, the wake transitions to the next regime, the P mode.

The P mode (figure 2, $\alpha = 9^{\circ}$) is distinguished by periodic von Kármán shedding of a single vortex pair (P represents a single vortex pair). The spatial separation between two vortex pairs is distinctly larger compared to that observed between the single vortices in the 2S mode. The time averaged vorticity contour lines of the regime shifts above the wake centerline, portraying decrease in lift growth with α . Height of the wake increases considerably compared to the 2S regime. This will increase the drag force experienced by the airfoil. The 2S and P modes are characterized by the occurrence of single peaks in the frequency spectra of lift data, which is discussed in the Appendix. Further increase in α and h/c values causes the wake transition to the complex 2P mode.

The 2P mode (figure 2, $\alpha = 15^{\circ}$) is characterized by two pairs of vortices convecting above and below the wake centerline. The time averaged vorticity field for the 2P regime evidently depicts the vortex pairs convecting towards two directions from the wake centerline. Compared to all other regimes, the wake is most prominent for the 2P regime. Consequently, the drag force experienced by the airfoils for this regime will be the highest compared to that of all the other modes. Also, the downward force acting on the airfoil due to the upward displacement of the mean flow reduces the lift growth with α . The frequency spectra of lift data for a case classified in the 2P regime exhibits two peaks, portraying the shedding of the two pairs of vortices. Further discussion on the spectral analysis on lift data is reported in the Appendix. The occurrence of the 2P mode is found in baseline cases (without Gurney flap) for NACA 0012 at Re = 1000 by Kurtulus, 11,12 but only at very high angles of attack, $\alpha \in [23^{\circ}, 41^{\circ}]$. By adding the flap, the 2P regime appears at lower α .

In summary, we use the observations and results to classify the wake regimes of all the airfoils using a wake classification diagram on the $(\alpha, h/c)$ plane. Figure 3 gives an account of the simulations performed and wake classification of the different cases analyzed. Representative vorticity fields of different wake regimes observed are also portrayed for each airfoil case. With the addition of the Gurney flap, transition of the unsteady wake modes occur earlier with respect to angle of attack. The wake classification diagram shifts towards the left axis of the $(\alpha, h/c)$ plane with increase in the Gurney flap height.

When the airfoil geometry is changed from flat plate to a thick airfoil, the occurrence of the 2P regime is delayed to higher h/c and α values. Also, size of the steady regime decreases. Increasing the thickness of the airfoil lead to a decrease in the effect of the Gurney flap. The thickness of the airfoil overshadows the effect of the flap when the thickness is increased. Thicker airfoils act more like a bluff body, and the influence of the Gurney flap is eclipsed. As a result of this, the complex 2P mode is revealed only at higher α and h/c values for thicker airfoils.

The wake classification diagram provides a broad picture of the effect of adding Gurney flap to the trailing edge of the airfoil. The diagram is useful to determine the nature of flow at different h/c and α values for all the airfoils studied. The overall performance of different airfoil-Gurney flap configurations can be understood from the diagram. This can be used to determine the optimal geometric and angle of attack conditions for different aerodynamic performance requirements. Depending on the necessity, the ideal airfoil

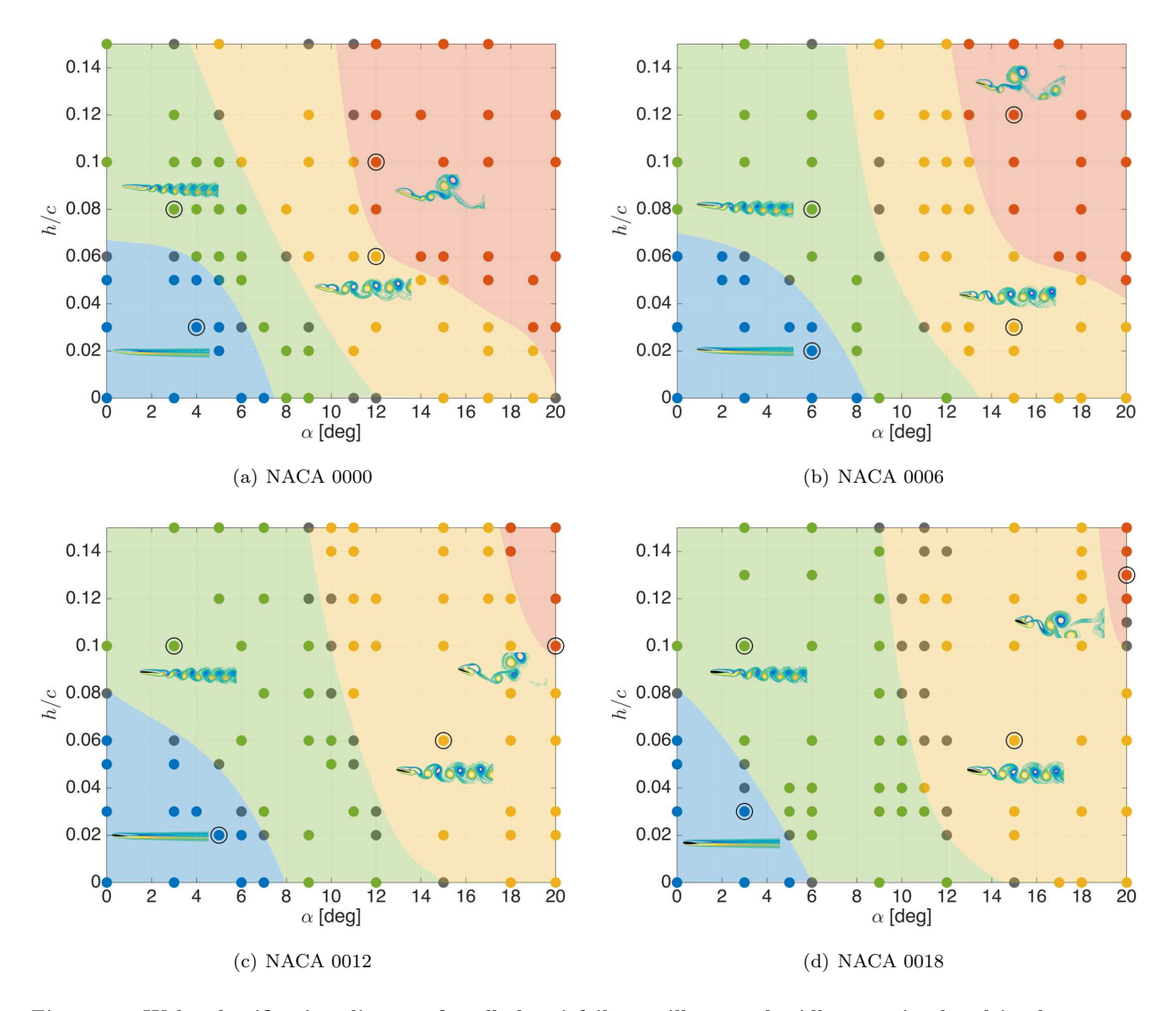


Figure 3. Wake classification diagram for all the airfoils are illustrated. All cases simulated in the current study are categorized into different characteristic wake regimes respect to h/c and α values. Different regimes are described by: steady - blue, 2S - green, P - yellow, 2P - red and transition between two regimes - gray. The boundaries for all the regimes are obtained by polynomial curve fitting. Representative vorticity field contour plots are also presented for each wake regime of all airfoils.

and corresponding Gurney flap configuration can be chosen.

B. Aerodynamic Forces

Next, we examine the effects of the wake modifications on aerodynamic characteristics of the airfoils. The main objective of attaching a Gurney flap to the trailing edge of an airfoil is to enhance the lift force experienced by the airfoil. Results of the current study show that at a low Reynolds number of Re = 1000, the Gurney flap is able to generate high levels of lift forces. It is also seen that as the height of the flap is increased, lift also increases. The lift coefficient, C_L , of representative cases for each airfoil is shown in figure 4, where the time-averaged values, $\overline{C_L}$, are depicted by the solid lines and the fluctuations in the forces are denoted by the shaded bands. The blue lines for h/c = 0.00 cases depict the baseline results without a Gurney flap for all the airfoils.

As discussed above, the results show that $\overline{C_L}$ increases with α and h/c values for all airfoils. Lift force enhancement of more than twice the baseline values is achieved using Gurney flap, particularly at h/c = 0.10 for all airfoils. Due to the presence of the Gurney flap, effective camber of the airfoil increases, attributing

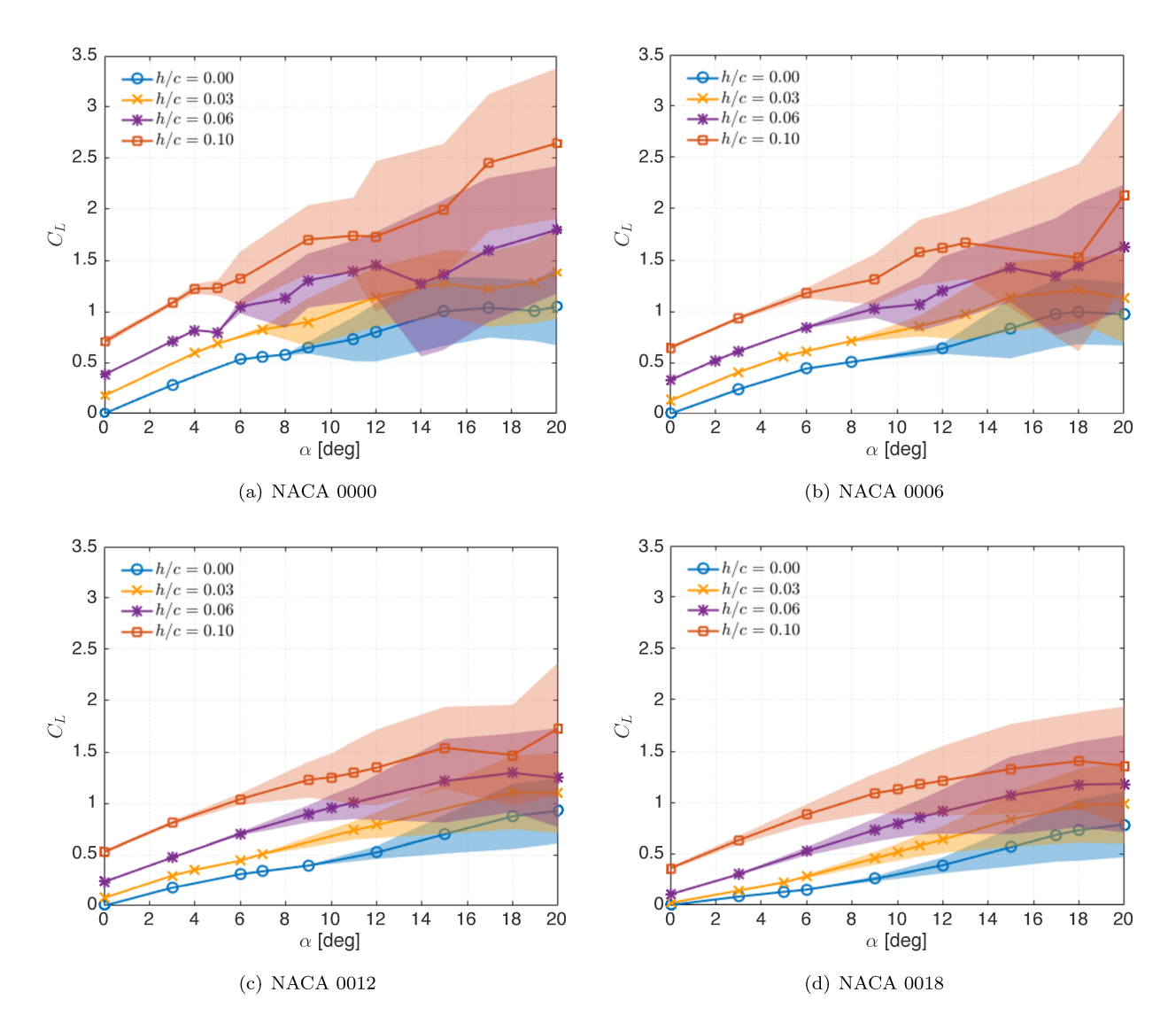


Figure 4. Lift coefficient C_L over angle of attack α for NACA 0000, 0006, 0012 and 0018 airfoils with select Gurney flap heights. The time-averaged $\overline{C_L}$ values are represented by the solid lines and fluctuations in C_L are represented by the shaded region for each configuration.

to lift enhancement. Fluctuations in the lift forces appear when the flow transitions from steady to unsteady state (2S regime). For a given angle of attack, $\overline{C_L}$ as well as the fluctuations of C_L are amplified with increase in Gurney flap height. A sudden jump or burst in C_L fluctuations are also observed for all the cases at high angles of attack. Therefore, the growth of the fluctuating forces exhibits trends of sudden increase in magnitude, suggesting a transition from one flow regime to another with different Gurney flap height and angles of attack. The transition corresponds to the wake mode shift from the P mode to the 2P mode. Thus, the airfoil experiences the highest magnitude of lift when the wake is classified under the 2P mode. The transition of the wake from the steady regime through the 2P regime can be evidently observed by the jagged growth of C_L fluctuations with α for the NACA 0000 airfoil.

The thickness of the airfoil plays a major role in the lift enhancement. As the thickness of the airfoil is increased from that of a flat plate (NACA 0000), lift decreases. The highest value of $\overline{C_L}$ at a given α is experienced by NACA 0000 and the lowest by NACA 0018. There is significant difference in the nature of growth of $\overline{C_L}$ with α for all the airfoils. For thinner airfoils (NACA 0000 and 0006), the growth is abrupt with increase in α and follow a more jagged trend, whereas the trend is much smoother for thicker airfoils (NACA 0012 and 0018), although the magnitude of $\overline{C_L}$ generated by thicker airfoils are lower compared to thinner airfoils. The same observation is made for C_L fluctuations. Another behavior which can be observed

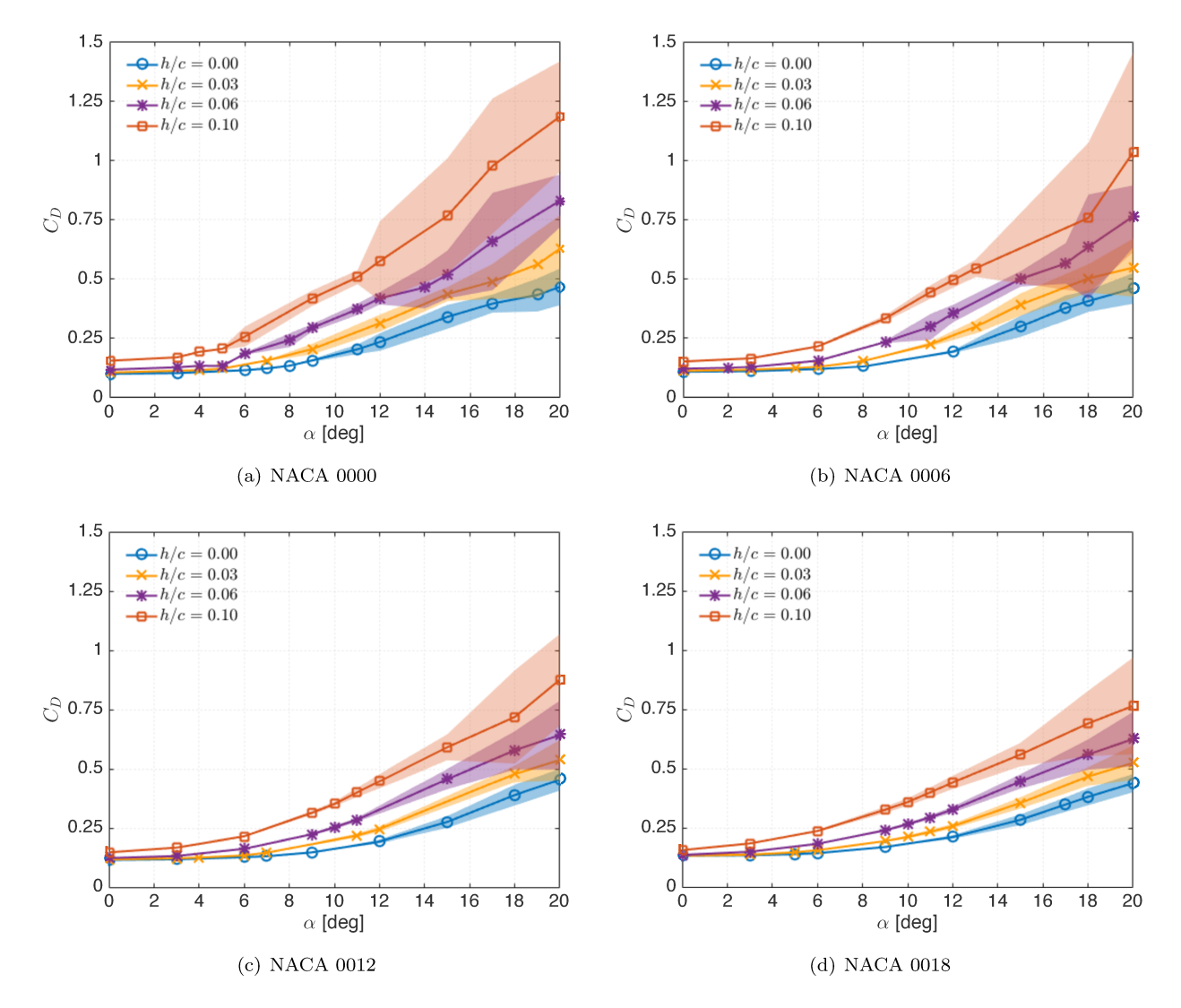


Figure 5. Drag coefficient C_D over angle of attack α for NACA 0000, 0006, 0012 and 0018 airfoils with select Gurney flap heights. The time-averaged $\overline{C_D}$ values are represented by the solid lines and fluctuations in C_D are represented by the shaded region for each configuration.

is the increase in lift forces at very high angle of attacks, $\alpha \in [15^{\circ}, 20^{\circ}]$. For thinner airfoils, the lift force continues to grow in this α range, whereas for thicker airfoils, the growth rate $(dC_L/d\alpha)$ decreases and flattens the lift curve (evident for NACA 0018 with h/c = 0.10 in figure 4).

The benefit of lift enhancement is however accompanied with a penalty of some drag increase. Figure 5 depicts the drag coefficient, C_D , of representative cases for each airfoils. As it can be observed, $\overline{C_D}$ increases with α and h/c values. The appearance of fluctuations in C_D in conjunction with the wake transition from the steady regime to the 2S regime is also observed at lower α , but the magnitudes of the fluctuations are very small. The sudden increase in the values of the fluctuations of drag at high α when the wake transition from the P mode to the 2P mode, previously observed for lift, is also clearly observable for all airfoils.

Next, we examine the effect of airfoil thickness on drag. As expected, for the baseline cases, C_D increases with increase in airfoil thickness. In contrast, with attachment of the Gurney flap, the trend reverses, particularly at high α . The aerodynamically fluidic or streamline shape of airfoils are reduced with the attachment of the Gurney flap to the trailing edge. The magnitude of increase in C_D with the attachment of Gurney flap is higher for thinner airfoils compared to thicker airfoils. This can be clearly observed at $\alpha = 0^{\circ}$ and h/c = 0.10 for all the airfoils. The increase in C_D is evident for NACA 0000 and 0006, whereas the magnitude of increment is negligible for NACA 0012 and 0018. This is due to the fact that with increase

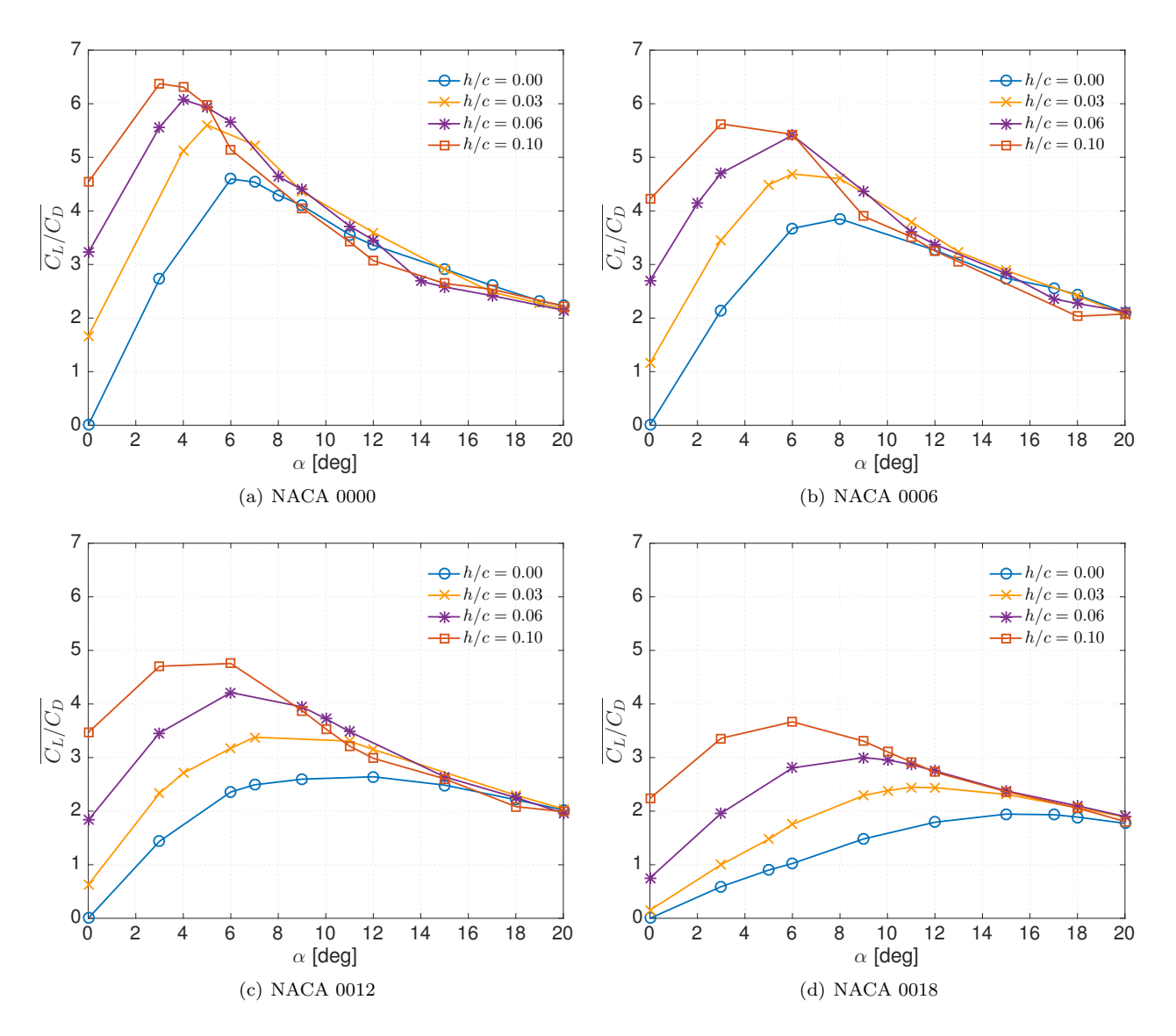


Figure 6. Lift-to-drag ratio $\overline{C_L/C_D}$ over angle of attack α for NACA 0000, 0006, 0012 and 0018 airfoils with Gurney flap.

in airfoil thickness, the effect of the Gurney flap is overshadowed. Thus, the drag added by the protruding Gurney flap at the trailing edge is decreased for thicker airfoils compared to thinner airfoils.

The aerodynamic efficiency of the airfoils are examined next. Lift-to-drag ratio (aerodynamic efficiency), $\overline{C_L/C_D}$, of all airfoils are depicted in figure 6. With increase in α , the efficiency growth is significant initially, reaches a peak and then decreases gradually. The enhancement of efficiency is achieved when the Gurney flap is attached to the trailing edge of the airfoils. The $\overline{C_L/C_D}$ at lower angles of attack, in the range of $\alpha \in [0^\circ, 12^\circ]$, is observed to be higher compared to baseline cases in general for all airfoils and flap heights. This range of α is smaller for thinner airfoils (NACA 0000 and 0006) although the peak value of $\overline{C_L/C_D}$ is higher compared to thicker airfoils (NACA 0012 and 0018). The flow is steady under this condition. At higher range of α , $\overline{C_L/C_D}$ decreases and reaches values close to the baseline values for the controlled cases of all airfoils. At higher α , the curves are slightly lower than the baseline cases for NACA 0000 and 0006 even though they have higher $\overline{C_L/C_D}$ magnitude at lower α compared to thicker airfoils. This corresponds to when the wake modes transition from steady to the 2P regime, where the airfoils experience the highest magnitude of drag. By comparing figures 4, 5 and 6, it can be noted that for each airfoil, the flow regime when the fall in $\overline{C_L/C_D}$ starts correspond to the 2S regime when fluctuations initiate for C_L and C_D .

All the above observations show that an airfoil with a large Gurney flap at high angles of attack experiences large forces. With increase in α , thinner airfoils (NACA 0000 and 0006) experience the highest levels of lift and drag, whereas thicker airfoils (NACA 0012 and 0018) experience shallower growth and fall of the forces over α . The enhanced lift-to-drag ratio brought about by the Gurney flap is maintained over a larger range of α and h/c values in thicker airfoils, while thinner airfoils experience higher magnitude of $\overline{C_L/C_D}$ over a shorter range of α . Thus, for high levels of lift generation and $\overline{C_L/C_D}$ requirements, thinner airfoils can be suitable amongst the considered airfoils. In contrast, to obtain the enhanced $\overline{C_L/C_D}$ over a wider range of angles of attack and lower drag when Gurney flap is attached, thicker airfoils perform well, although with a relatively lower magnitude of $\overline{C_L/C_D}$.

IV. Concluding Remarks

Two-dimensional direct numerical simulations are performed for incompressible flow at Re=1000 over different airfoils - NACA 0000, 0006, 0012 and 0018, with and without a Gurney flap attached to the trailing edge. Adding a Gurney flap to the airfoils enhances the lift force experienced by the airfoils, and their aerodynamic efficiency. With increase in airfoil thickness, $dC_L/d\alpha$ and $\overline{C_L/C_D}$ decreases, whereas drag force grows. When the forces are compared between baseline models and models subjected to high α and h/c values, a modest increase in the lift force and $\overline{C_L/C_D}$ is observed for thicker airfoils (NACA 0012 and 0018). Also, drag force on the airfoils reduces at higher α comparatively for thicker airfoils.

A close observation of the flow field, force data and frequency spectra reveals the evolution of different characteristic vortex shedding patterns from the airfoil body. These are classified into four regimes: (1) steady, (2) 2S - periodic von Kármán vortex shedding of alternate counter-clockwise and clockwise rotating vortices, (3) P - transition stage with periodic von Kármán shedding of a vortex pair and (4) 2P - periodic complex von Kármán shedding of two vortex pairs. Study on the wake classification of all the cases revealed that with increase in α and h/c values, the wake shifts from steady regime through the 2P regime. Spectral analysis reveals distinct Strouhal number values for the dominant vortex shedding frequency for different regimes. St values fall in the range between 0.16 and 0.18 for cases in 2S and P regime, and between 0.06 and 0.1 for flows characterized under 2P regime. The wake type and St number trends are observed consistently for all airfoils and can be used as characteristic properties to determine the wake type of an airfoil configuration.

Airfoil thickness is an important factor determining the performance of the airfoil-Gurney flap configuration. With increase in airfoil thickness, the flow is more likely to be unsteady. This is due to the fact that with increase in airfoil thickness, the airfoil behaves more like a bluff body, where flow becomes unsteady very rapidly with increase of α . Occurrence of the 2P regime is also suppressed with increase in airfoil thickness. For larger airfoil thickness, the effect of the Gurney flap is overshadowed by the airfoil profile. This also explains the comparative increase in airfoil performance at high α conditions for thicker airfoils at larger h/c values. Majority of the cases for thicker airfoils fall under 2S and P regimes, showing that the vortex shedding phenomena starts to follow more of 2S and P trends, and less of complex 2P type shedding.

In summary, we observed that <u>airfoils</u> with Gurney flaps attached to the trailing edge experiences large increase in aerodynamic efficiency $\overline{C_L/C_D}$, at low Reynolds number of Re=1000. At high angles of attack and with increasing Gurney flap height, the efficiency is reduced. Thinner airfoils underperform compared to their respective baseline models. On the other hand, thicker airfoils are able to sustain efficiencies comparable to their baseline models at such configurations. Four different wake modes are found for all airfoils, which can be classified based on the vortex shedding pattern and St corresponding to the dominant shedding mode. Performance of the airfoil can be judged depending on the nature of wake regime the respective flow is classified under for the particular angle of attack and flap height.

Appendix

Spectral Analysis

Results of the spectral analysis conducted on the lift history are discussed to gain additional insights on the unsteady nature of lift and drag of the airfoil-Gurney flap configurations. The changes in unsteady component of lift and drag are caused by the airfoil wake transitioning into different unsteady, complex flow regimes. Thus, it is important to understand the nature of the wake by analyzing the vortex shedding

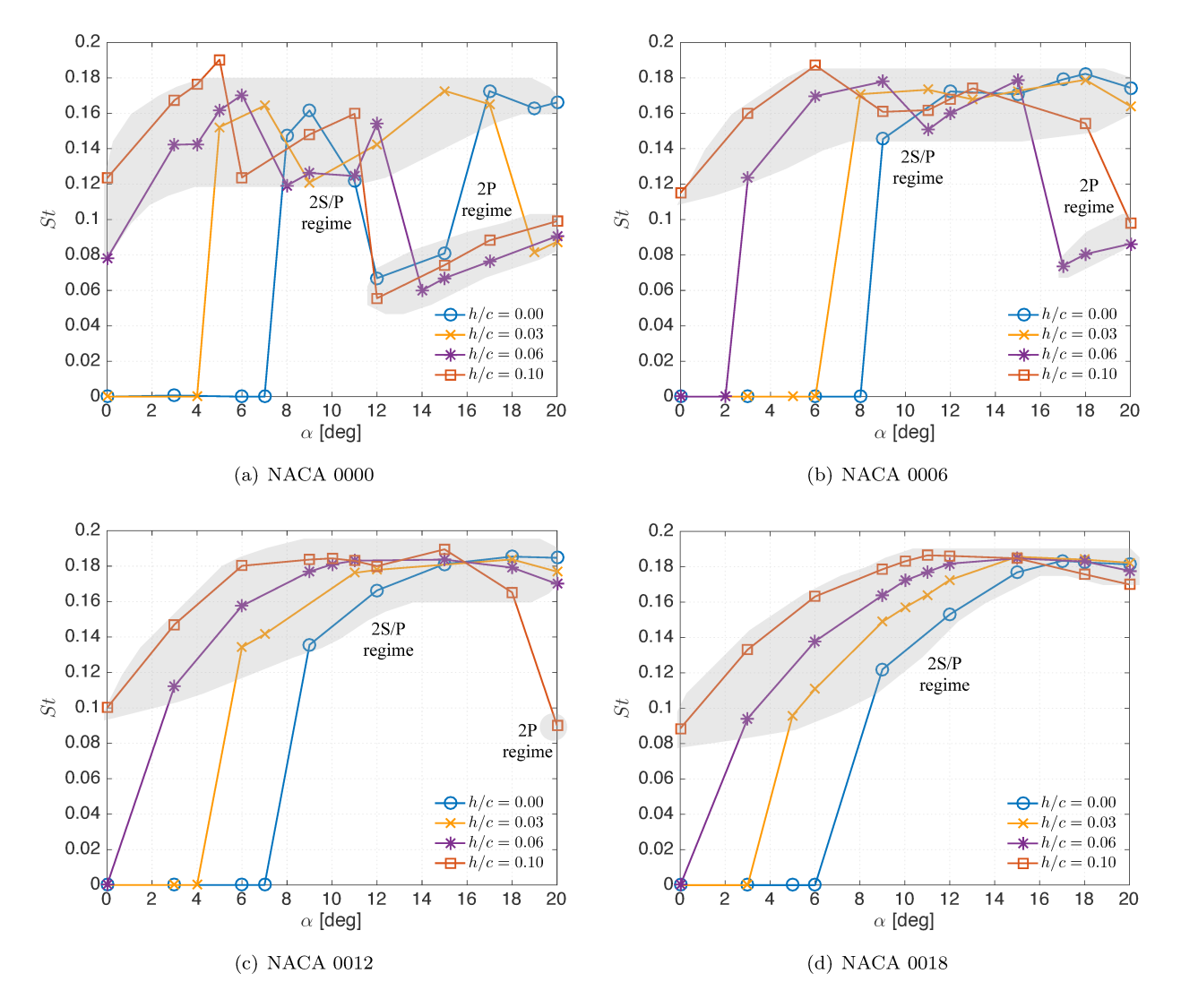


Figure 7. Dominant vortex shedding frequency in terms of Strouhal number St over angle of attack α for NACA 0000, 0006, 0012 and 0018 airfoils with select Gurney flap heights. Regions with $St \in [0.12, 0.18]$ are classified as 2S and P regimes, and $St \in [0.06, 0.10]$ as 2P regime, depicted by the gray shaded regions.

phenomena over a broad range of flow regimes. After the flow transitions from steady to unsteady regime, two dominant peaks in the lift spectra are observed revealing vortex shedding modes. These modes are examined in the following section, with the flow regimes being classified into 2S, P and 2P.

The dominant peak in the lift spectra corresponds to the vortex shedding frequency and is called the shedding mode. The dominant vortex shedding frequencies, non-dimensionalized as Strouhal number using Eq. (2), are plotted versus angle of attack for all the airfoils in figure 7. With increase in α , the dominant shedding frequency grows rapidly from zero value, when the flow transitions from steady to unsteady state, and saturates to a peak values of $St \in [0.12, 0.18]$. This represents the wake mode classified under the 2S and the P regimes. At higher α , the St values drop sharply and saturates at values $St \in [0.06, 0.1]$, representing the 2P regime. The two sets of St values further signifies the existence of characteristic flow regimes in the flow past the airfoil-Gurney flap configuration at different geometric setups and at Re = 1000. Therefore, apart from the flow field visualization method, the Strouhal number value corresponding to the shedding mode for a case is used as one of the criteria to classify the airfoil wakes into different modes, 2S, P and 2P.

Energy spectral density of the shedding mode, defined by $\widehat{C_L}_{\text{shedding}}^2$, is also analyzed in the study by the authors, and is noticed to increase with Gurney flap height and angle of attack. The value grows in the flow regime where $St \in [0.12, 0.18]$ and abruptly reaches high magnitudes at the regime where $St \in [0.06, 0.1]$,

again imposing the significance of the two characteristic Strouhal number regimes. The observations suggest that the size of the vortex structure being shed increases when the flow transitions from the 2S and P modes to the 2P mode, while the time period by which the structure sheds increases.

The second prominent peak observed from the spectral analysis are harmonics of the respective dominant frequencies. For flow regimes with the shedding mode having $St \in [0.06, 0.1]$ (2P regime), harmonic frequencies in periodic shedding range of $St \in [0.1, 0.2]$, are observed. This implies that secondary vortex shedding phenomena is prominent in the 2P mode, which is evident from the two pairs of vortices observed in the wake of the 2P mode previously depicted in figure 2.

The energy spectral density for the subharmonic mode is studied by taking the ratio of energy spectral density of subharmonic mode to that of the shedding mode, $\widehat{C_L}_{\text{subharmonic}}^2/\widehat{C_L}_{\text{shedding}}^2$. The ratio has very low values initially, but grows abruptly over high α . This is observed mostly in the 2P regime where evidence of secondary vortex shedding is observed. Abrupt increase in the values of the energy spectral density observed for the 2P regime shows the fact that secondary vortices have important effects on the force experienced by the airfoil in this regime. In the current study, subharmonic modes with energy ratio values greater than a threshold value of 0.1 are only considered to be significant.

Acknowledgments

The authors thank the insightful discussions with Daisuke Oshiyama and Phillip Munday. The majority of the computation for this project was performed at the Research Computing Center at the Florida State University. MGM and KT were partially supported by the National Science Foundation (Award Number 1632003).

References

- ¹Liebeck, R. H., "Design of subsonic airfoils for high lift," Journal of Aircraft, Vol. 15, No. 9, 1978, pp. 547–561.
- ²Katz, J. and Largman, R., "Effect of 90 degree flap on the aerodynamics of a two element airfoil," *Journal of Fluids Engineering*, Vol. 111, No. 1, 1989, pp. 93–94.
- 3 Neuhart, D. H. and Pendergraft Jr, O. C., "A water tunnel study of Gurney flaps," NASA Technical Memorandum 4071, 1988.
- ⁴Jang, C. S., Ross, J. C., and Cummings, R. M., "Numerical investigation of an airfoil with a Gurney flap," *Aircraft Design*, Vol. 1, No. 2, 1998, pp. 75.
- ⁵Jeffrey, D., Zhang, X., and Hurst, D. W., "Aerodynamics of Gurney flaps on a single-element high-lift wing," *Journal of Aircraft*, Vol. 37, No. 2, 2000, pp. 295–301.
- ⁶Li, Y., Wang, J., and Zhang, P., "Effects of Gurney flaps on a NACA0012 airfoil," Flow, Turbulence and Combustion, Vol. 68, No. 1, 2002, pp. 27–39.
- ⁷Oshiyama, D., Numata, D., and Asai, K., "Lift-Enhancing Mechanism of Mini Flaps at Low Reynolds Number," *The Japan Society for Aeronautical and Space Science 2015-D12-1087*, 2015.
- ⁸Zhang, P., Liu, A., and Wang, J., "Aerodynamic modification of NACA 0012 airfoil by trailing-edge plasma gurney flap," *AIAA Journal*, Vol. 47, No. 10, 2009, pp. 2467–2474.
- ⁹Feng, L.-H., Choi, K.-S., and Wang, J.-J., "Flow control over an airfoil using virtual Gurney flaps," *Journal of Fluid Mechanics*, Vol. 767, 2015, pp. 595–626.
- ¹⁰Mittal, S. and Tezduyar, T. E., "Massively parallel finite element computation of incompressible flows involving fluid-body interactions," *Computer Methods in Applied Mechanics and Engineering*, Vol. 112, No. 1-4, 1994, pp. 253–282.
- 11 Kurtulus, D. F., "On the unsteady behavior of the flow around NACA 0012 airfoil with steady external conditions at Re = 1000," International Journal of Micro Air Vehicles, Vol. 7, No. 3, 2015, pp. 301–326.
- 12 Kurtulus, D. F., "On the wake pattern of symmetric airfoils for different incidence angles at Re = 1000," International Journal of Micro Air Vehicles, Vol. 8, No. 2, 2016, pp. 109–139.
- ¹³Mateescu, D., Panahi, A., and Roy, V., "Analysis of the flow past airfoils with Gurney flaps at low Reynolds numbers," AIAA Paper 2014-0040, 2014.
- ¹⁴Taira, K. and Colonius, T., "The immersed boundary method: a projection approach," J. Comput. Phys., Vol. 225, 2007, pp. 2118–2137
- ¹⁵Colonius, T. and Taira, K., "A fast immersed boundary method using a nullspace approach and multi-domain far-field boundary conditions," *Comput. Methods Appl. Mech. Engrg.*, Vol. 197, 2008, pp. 2131–2146.
- ¹⁶Hoarau, Y., Braza, M., Ventikos, Y., Faghani, D., and Tzabiras, G., "Organized modes and the three-dimensional transition to turbulence in the incompressible flow around a NACA0012 wing," *Journal of Fluid Mechanics*, Vol. 496, 2003, pp. 63–72.
- 17 Suzuki, T., Ji, H., and Yamamoto, F., "Unsteady PTV velocity field past an airfoil solved with DNS: Part 1. Algorithm of hybrid simulation and hybrid velocity field at $Re \approx 10^3$," Experiments in Fluids, Vol. 47, No. 6, 2009, pp. 977–994.
 - ¹⁸Liu, Y., Li, K., Zhang, J., Wang, H., and Liu, L., "Numerical bifurcation analysis of static stall of airfoil and dynamic

stall under unsteady perturbation," Communications in Nonlinear Science and Numerical Simulation, Vol. 17, No. 8, 2012, pp. 3427–3434.

 $^{19}\mbox{Williamson},$ C. H. K. and Roshko, A., "Vortex formation in the wake of an oscillating cylinder," J. Fluids Struc., Vol. 2, 1988, pp. 355–381.

²⁰Griffin, O. M. and Ramberg, S. E., "Vortex shedding from a cylinder vibrating in line with an incident uniform flow," *Journal of Fluid Mechanics*, Vol. 75, No. 02, 1976, pp. 257–271.

 $^{21}\mathrm{Ongoren},$ A. and Rockwell, D., "Flow structure from an oscillating cylinder Part 2. Mode competition in the near wake," *Journal of Fluid Mechanics*, Vol. 191, 6 1988, pp. 225–245.

²²Brika, D. and Laneville, A., "Vortex-induced vibrations of a long flexible circular cylinder," *Journal of Fluid Mechanics*, Vol. 250, 1993, pp. 481–481.

²³Williamson, C. and Govardhan, R., "Vortex-induced vibrations," Annu. Rev. Fluid Mech., Vol. 36, 2004, pp. 413–455.

²⁴Singh, S. and Mittal, S., "Vortex-induced oscillations at low Reynolds numbers: hysteresis and vortex-shedding modes," *Journal of Fluids and Structures*, Vol. 20, No. 8, 2005, pp. 1085–1104.

 25 Bratt, J. B., "Flow patterns in the wake of an oscillating aerofoil," A.R.C Reports and Memoranda No. 2773, Her Majesty's Stationery Office, 1953.

²⁶Koochesfahani, M. M., "Vortical patterns in the wake of an oscillating airfoil," AIAA Journal, Vol. 27, No. 9, 1989, pp. 1200–1205.

²⁷Jones, K., Dohring, C., and Platzer, M., "Wake structures behind plunging airfoils: a comparison of numerical and experimental results," *AIAA paper 1996-0078*, 1996.